

Electronic Supplementary Information

Porous Microspheres of MgO-Patched TiO₂ for CO₂ Photoreduction with H₂O Vapor: Temperature-Dependent Activity and Stability

Lianjun Liu,^a Cunyu Zhao,^a Huilei Zhao,^a Daniel Pitts,^a Ying Li^{*a}

Mechanical Engineering Department, University of Wisconsin-Milwaukee, Milwaukee, Wisconsin 53211, USA.

Fax: (+1) 414-229-6958;

Tel: (+1) 414-229-3716;

E-mail: liying@uwm.edu

1. Experiment

1.1 Catalyst preparation

MgO/TiO₂ microsphere composites were prepared by an ultrasonic spray pyrolysis (USP) process, similar to that reported in our previous study.¹ The apparatus and the formation mechanism were shown in Figure S1. The spraying solution was prepared by mixing an aqueous Mg(NO₃)₂ solution and TiO₂ (Degussa P25) nanoparticles and sonicating for 30 min. The TiO₂ concentration was fixed at 16 mg/ml and the amount of Mg(NO₃)₂ was calculated according to the atomic percentage of Mg to Ti (i.e., 20%) in the catalysts. The ultrasonic nebulizer (Sonaer) has a frequency of 2.4 MHz and produces droplets with a volumetric mean diameter of 1.8 μm. The generated fine mists containing Mg(NO₃)₂/TiO₂ were carried out by nitrogen gas and passed through a diffusion dryer composed of silica gels where the solvent (i.e., water) evaporated and Mg(NO₃)₂ concentrated on the surface of TiO₂ particles. The particles then passed through a cylindrical quartz reactor that was placed inside a tube furnace (Thermo Fisher) with a set temperature of 500 °C. The Mg(NO₃)₂ was thermally decomposed and deposited on the surface of TiO₂ forming MgO/TiO₂ microsphere composites. The spray-pyrolyzed particles were collected on a glass fiber filter placed inside a stainless-steel filter holder.

Pure TiO₂ sample was also prepared using the same USP method without the addition of Mg(NO₃)₂. Al₂O₃/TiO₂ was prepared by the same USP method with the addition of Al(NO₃)₃, and the atomic ratio of Al:Ti was 5%. CuO/TiO₂ was prepared by a wet-impregnation method with Cu(NO₃)₂ and TiO₂-P25. The atomic ratio of Cu:Ti was 1%. The resulting powders were finally calcined at 400 °C for 2 h.

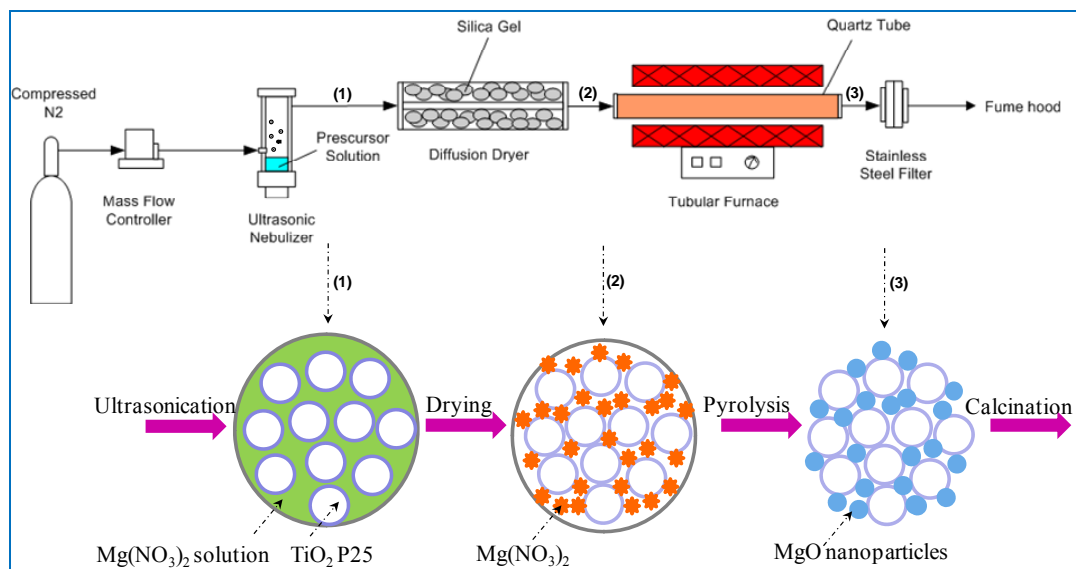


Figure S1. Schematic diagram of the ultrasonic spray pyrolysis process and the formation mechanism of MgO/TiO₂ porous microspheres

1.2 Catalyst characterization

The crystal structures of the TiO₂, MgO/TiO₂, CuO/TiO₂ and Al₂O₃/TiO₂ samples were identified by X-ray diffraction (XRD, Scintag XDS 2000) using Cu K α irradiation at 45 kV and a diffracted beam monochromator at 40 mA. The surface area, pore size and pore volume of TiO₂, MgO/TiO₂, CuO/TiO₂ and Al₂O₃/TiO₂ were analyzed by nitrogen adsorption-desorption at 77 K using the Brunauer-Emmett-Teller (BET) method (Micromeritics, ASAP 2020). The UV-vis diffuse reflectance spectra were obtained by a UV-vis spectrometer (Ocean Optics) using BaSO₄ as the background. Scanning electron microscopy (SEM) (Hitachi S4800) was used to obtain the catalysts surface morphology. The dispersion of elements (Mg, Ti, O) on TiO₂ and MgO/TiO₂ was analyzed by X-ray elemental mapping (XREM). The lattice structures of CuO/TiO₂ and MgO/TiO₂ were visualized by phase-contrast high resolution transmission electron microscopy (HRTEM) carried out with 300 keV electrons in a Hitachi H9000NAR instrument with 0.18 nm point and 0.11 nm lattice resolution. Amplitude contrast TEM images were used to obtain the information about the sizes and morphology.

1.3 In situ DRIFTS for reactant adsorption and intermediate/product desorption

All IR spectra were recorded on a Nicolet 6700 spectrometer (Thermo Electron) equipped with a liquid nitrogen cooled HgCdTe (MCT) detector. The spectra were displayed in absorbance units, and acquired with a resolution of 4 cm⁻¹, using 32 scans. The DRIFTS studies were performed in a Praying Mantis DRIFTS accessory and a reaction chamber (Harrick Scientific, HVC-DRP). The reaction cell is equipped with a heater and a temperature controller, as well as a sample cup in the center. The dome of the DRIFTS cell has two KBr windows allowing IR transmission and a third (quartz) window allowing transmission of irradiation introduced through a liquid light guide (Newport) that connects to a 450 W Xe lamp (Oriel).

The reactant (e.g., CO₂ and H₂O) adsorption on the catalyst surface was studied by introducing a CO₂/H₂O mixture to the IR cell. Prior to the adsorption, the samples were purged by He for 1 h at 300 °C. After the temperature was cooled down to 50 °C, the background spectrum in the presence of the sample was collected. For CO₂/H₂O co-adsorption, CO₂ passed through water bubbler to bring a mixture of CO₂/H₂O vapor into the chamber at 2.0 ml/min. Meanwhile, the IR spectra were recorded as a function of time (0 – 35 min) when the adsorption process reaches the saturation level. For the property of desorption, the experiments were firstly conducted by purging the catalyst surface with He for 30 min to investigate physi-desorption of surface species. Subsequently, the UV light was turned on for 45 min to investigate chemi-desorption of photocatalytic reaction intermediates/products (e.g., carbonate and bicarbonate).

Similar procedure was also conducted at 150 °C to investigate the dynamics of the reactant adsorption and intermediates desorption.

1.4 Photocatalytic activity measurement

The experiments of CO₂ photoreduction with H₂O on TiO₂ and MgO/TiO₂ catalysts were carried out in a photoreactor system.¹ For each test, 30 mg of catalysts were used and dispersed on a glass fiber inside the reactor. CO₂ continuously passed through a water bubbler to bring a mixed gas of CO₂+H₂O into the photoreactor at a flow rate of 2.0 ml/min. A 400 W Xe lamp (Oriel) was used as the light source, and the light intensity is about 420 mW/cm² in the range of 200 ~ 1000 nm. The light spectrum can be found in our previous publication.² The light irradiation from the Xe lamp resulted in a temperature at approximately 50 °C inside the photoreactor, measured by a thermocouple. To increase the reaction temperature to the range of 80 – 170 °C, a 250 W infrared lamp was used to heat up the photoreactor from the back (the housing of the reactor is stainless steel). The gaseous products in the reactor effluent were continuously analyzed by a gas chromatograph (GC, Agilent 7890A) equipped with both a thermal conductivity detector (TCD) and flame ionization detector (FID).

2. Results and discussion

Table S1. The BET surface area, pore volume, pore size and band gap of the TiO₂, MgO/TiO₂, Al₂O₃/TiO₂ and CuO/TiO₂ catalysts

Samples	BET surface area (m ² /g)	Pore volume (cm ³ /g)	Pore size (nm)	Band gap (eV)
TiO ₂	52.1	0.241	18.5	3.19
MgO/TiO ₂	45.1	0.249	21.9	3.23
Al ₂ O ₃ /TiO ₂	50.7	0.249	19.7	3.22
CuO/TiO ₂	51.1	0.246	19.2	3.04

The BET surface areas of TiO₂, Al₂O₃/TiO₂ and CuO/TiO₂ were comparable, slightly higher than MgO/TiO₂. The pore volumes of the four catalysts were similar. While TiO₂ had the smallest pore size, MgO/TiO₂ had the largest pore size. The band gaps of TiO₂, Al₂O₃/TiO₂ and MgO/TiO₂ were comparable, slightly larger than that of CuO/TiO₂.

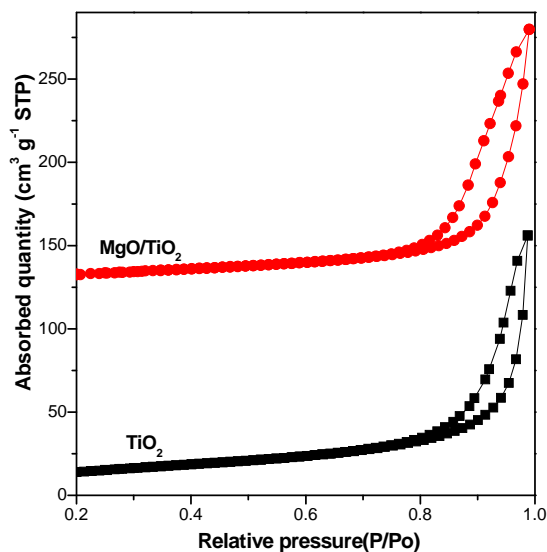


Figure S2. N₂ sorption/desorption isotherms for TiO₂ and Mg/TiO₂

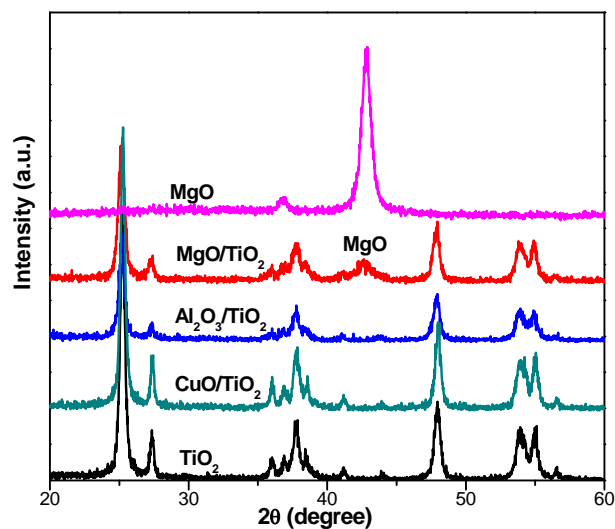


Figure S3. XRD patterns of TiO₂, CuO/TiO₂, Al₂O₃/TiO₂, MgO/TiO₂ and MgO samples

No CuO and Al₂O₃ crystals were found in CuO/TiO₂ and Al₂O₃/TiO₂, possibly due to their well dispersion or the low concentration (1.0 at% and 5.0 at%, respectively).

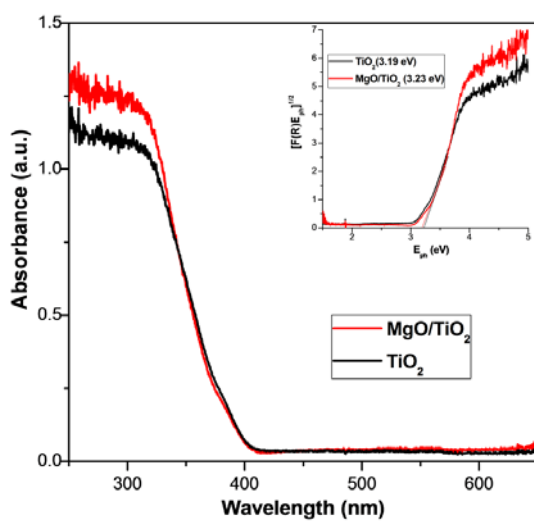


Figure S4. UV-vis spectra for TiO₂ and MgO/TiO₂, and the inset are the band gap analysis

The absorption edges of bare TiO₂ and MgO/TiO₂ were around 400 nm, corresponding to a similar calculated band gap of 3.19 and 3.23 eV, respectively. Compared to TiO₂, however, the light absorption was slightly enhanced on MgO/TiO₂ in the UV region, maybe because the dispersed MgO nanopatches on the TiO₂ surface could increase the scattering of light.

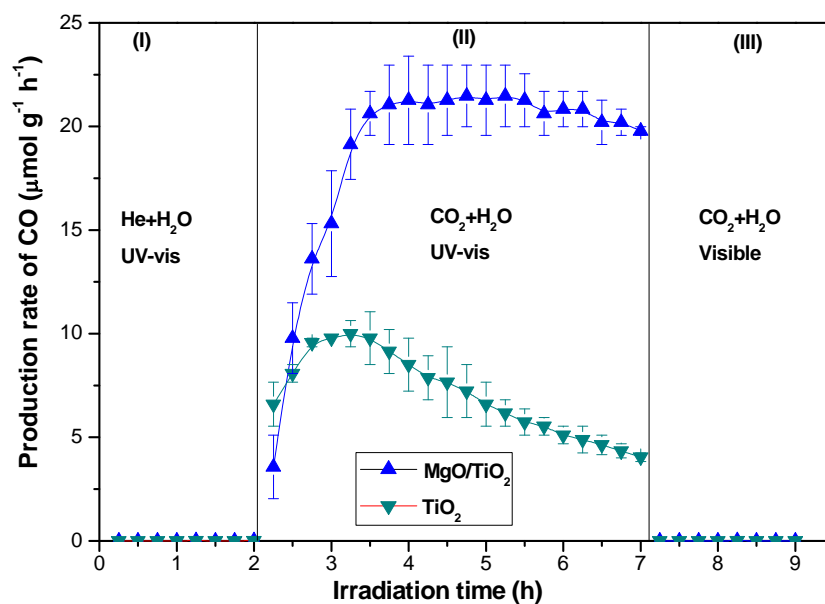


Figure S5. The production rate of CO on TiO₂ and MgO/TiO₂ at 150 °C: (I) helium + H₂O (without CO₂) under the UV-vis light irradiation, (II) CO₂ + H₂O under the UV-vis light irradiation for two independent runs, and (III) CO₂ + H₂O under only visible light irradiation.

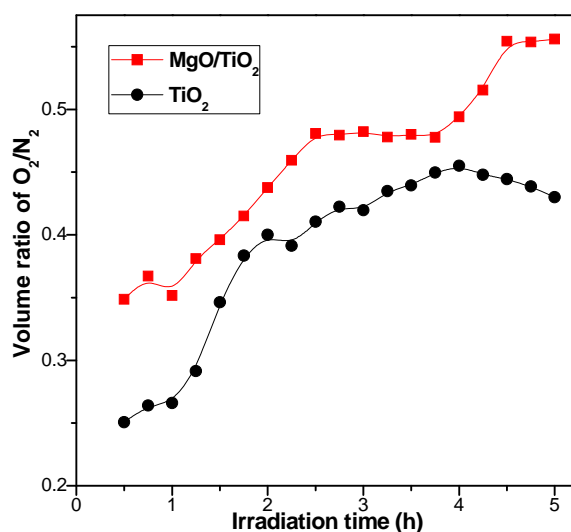


Figure S6. Time dependence of the volumetric ratio of O₂/N₂ during CO₂ photoreduction with H₂O on TiO₂ and MgO/TiO₂ at 150 °C

The production of O₂ from H₂O oxidation was measured for TiO₂ and MgO/TiO₂ catalysts during the CO₂ photoreduction experiments operated at 150 °C. Before turning on the UV-vis illumination, the photoreactor was purged with a CO₂+H₂O flow to remove air inside the reactor. However, there was always background O₂ and N₂ in the order of a few hundred ppm detected in the reactor effluent gas even after purging for a few hours. Hence, a better indicator of O₂ production by the catalyst is the volumetric ratio of O₂/N₂, as also reported in our previous work^{2,3} and a recent publication.⁴ As shown in Figure S6, the O₂/N₂ ratio gradually increased after 0.5 h photoillumination of TiO₂ and MgO/TiO₂, suggesting the generation of O₂ through oxidation of H₂O by photogenerated holes (i.e., H₂O + h⁺ → 2H⁺ + 1/2O₂, [R1]). After 3.5 h photoillumination, the O₂/N₂ ratio continued to increase on MgO/TiO₂; by contrast, the O₂/N₂ ratio on TiO₂ gradually decreased after 3.75 h. The O₂/N₂ ratio by MgO/TiO₂ was always larger than by TiO₂. This result suggested that MgO/TiO₂ was more active than TiO₂ for O₂ production, probably because of the enhancement on the adsorption of H₂O by MgO modification as evidenced by the TGA results (see Figure S8).

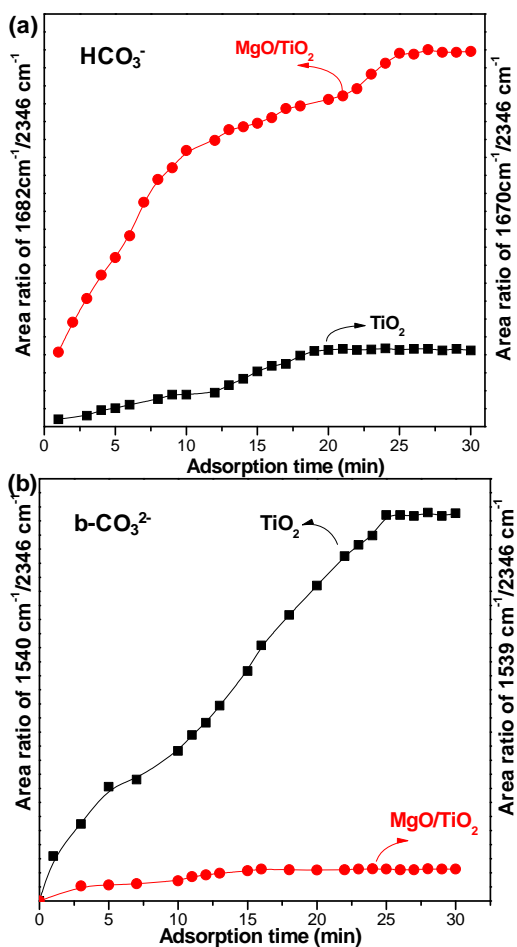


Figure S7. Time dependence of the ratio of (a) the peak area of HCO₃⁻ (1670-1682 cm⁻¹) and (b) the peak area of b-CO₃²⁻ (1540 cm⁻¹) to gaseous CO₂ (2346 cm⁻¹) in the DRIFTS spectra over the TiO₂ and MgO/TiO₂ catalysts.

The extent of HCO₃⁻ formation on TiO₂ versus MgO/TiO₂ is quantified by normalizing the peak area of HCO₃⁻ in the 1670-1682 cm⁻¹ range by that of the gaseous CO₂ peak at 2346 cm⁻¹ (i.e., peak area of HCO₃⁻/peak area of CO₂), since the gaseous CO₂ concentration remained relatively constant. As shown in Figure S7a, the ratio of HCO₃⁻ peak to CO₂ peak on MgO/TiO₂ was much higher than on TiO₂. At the early stage (1-15 min), the formation of HCO₃⁻ was at a faster rate (a large slope) on MgO/TiO₂ than on TiO₂. This result indicates that more HCO₃⁻ is formed on the MgO/TiO₂ surface. Similarly, we have also plotted the ratio of the peak area of b-CO₃²⁻ (1540 cm⁻¹) to gaseous CO₂ (2346 cm⁻¹) on the TiO₂ and MgO/TiO₂ catalysts (see Figure S7b). Opposite to the observation for the HCO₃⁻ peak, the b-CO₃²⁻ peak was much stronger on TiO₂ than on MgO/TiO₂.

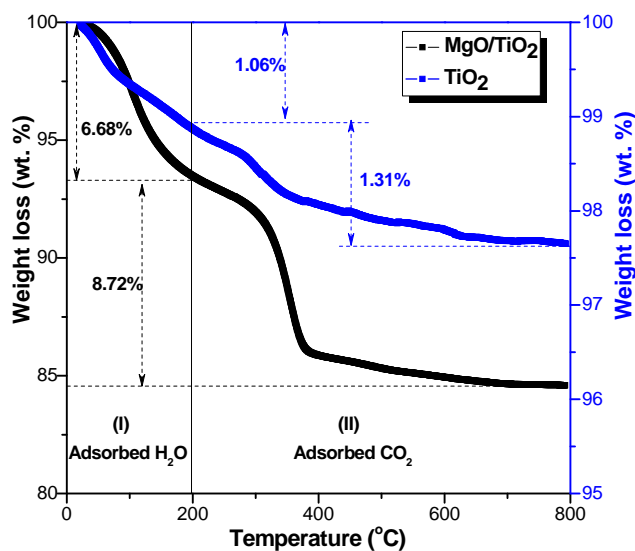


Figure S8. TGA profiles for the desorption of adsorbed CO₂ and H₂O from TiO₂ and MgO/TiO₂ after CO₂ and H₂O adsorption at 150 °C for 1 h

Thermal gravimetric analysis (TGA) was performed to investigate the effect of MgO modification on both H₂O and CO₂ adsorption. The sequence of experimental procedure was: (1) CO₂ and H₂O adsorption on the catalyst (TiO₂ or MgO/TiO₂) at 150 °C for 1 h; (2) cooling down the temperature to room temperature, and (3) desorption in an air flow in the range of 20 °C to 800 °C. The TGA profiles in the desorption step were shown in Figure S8. The weight loss in regions (I) and (II) was due to the removal of adsorbed H₂O and CO₂, respectively. Obviously, the weight loss of both adsorbed H₂O and CO₂ from MgO/TiO₂ (6.68% and 8.72%, respectively) was higher than that from TiO₂ (1.06% and 1.31%, respectively). This result demonstrated that MgO modification promoted the adsorption of both H₂O and CO₂, because MgO has a hygroscopic nature and abundant hydroxyl groups.⁵ The TGA results were consistent with the in situ DRIFTS analysis that MgO enhanced the formation of HCO₃⁻ species (Figure 3 in the main text).

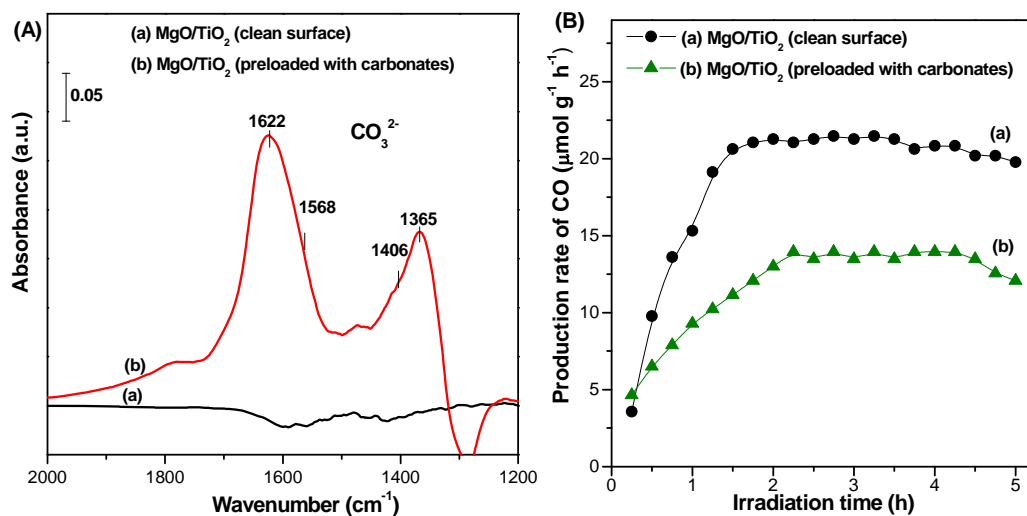


Figure S9. (A) FTIR spectra for MgO/TiO₂ (clean surface) and MgO/TiO₂ preloaded with carbonates; (B) The rate of CO production from CO₂ photoreduction with H₂O at 150 °C under UV-vis light irradiation on MgO/TiO₂ (clean surface) and MgO/TiO₂ preloaded with carbonates.

To intentionally poison MgO/TiO₂, we exposed MgO/TiO₂ to a flow of dry CO₂ at 400 °C for 2 h. It is noted that exposure of MgO/TiO₂ to moisturized CO₂ at lower temperatures (Figure 3b in the main text) resulted in the formation of dominating bicarbonate species and minor carbonate species. By contrast, exposure of MgO/TiO₂ to dry CO₂ at 400 °C leads to the formation of mainly carbonate species, as evidenced in the FTIR spectra shown in Figure S9A. The formed carbonate species are bidentate carbonates at 1622 and 1365 cm⁻¹ and monodentate carbonates at 1568 and 1406 cm⁻¹ [6-8].

The photocatalytic activity of the MgO/TiO₂ preloaded with carbonates was measured for CO₂ photoreduction with H₂O at 150 °C, and the result was compared with that obtained on the clean MgO/TiO₂ catalyst (Figure S9B). It is clear that both the initial rates (during the first 2 h) and the steady-state rate (after 2 h) of CO production on the clean MgO/TiO₂ are significantly higher than those on the MgO/TiO₂ preloaded with carbonates. This result confirmed that carbonate species have poisoning effect to the catalyst, most likely by occupying the surface active sites.

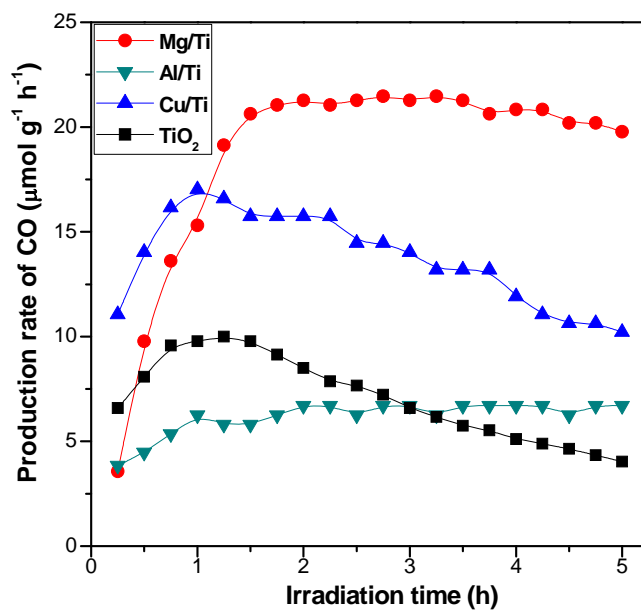


Figure S10. Comparison of the production rate of CO on TiO_2 , MgO/TiO_2 (Mg/Ti), CuO/TiO_2 (Cu/Ti) and $\text{Al}_2\text{O}_3/\text{TiO}_2$ (Al/Ti) at 150°C

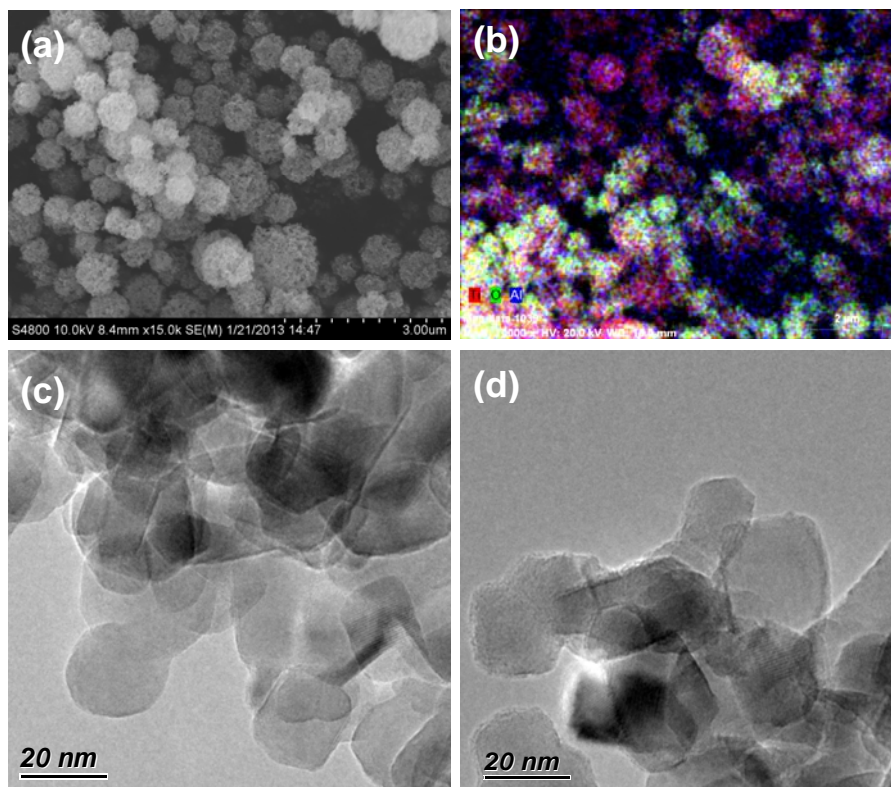


Figure S11. (a) SEM image and (b) X-ray elemental mapping image for $\text{Al}_2\text{O}_3/\text{TiO}_2$, and TEM images for (c) CuO/TiO_2 , and (d) MgO/TiO_2

The average diameter of $\text{Al}_2\text{O}_3/\text{TiO}_2$ microspheres was about $0.7 \mu\text{m}$ (Figure S11a). Similar to MgO/TiO_2 , the elemental mapping image of $\text{Al}_2\text{O}_3/\text{TiO}_2$ (Figure S11b) showed that Al_2O_3 particles were patched on the surface of TiO_2 spheres. The TEM images in Figure S11c-d demonstrated that the individual particles size of CuO/TiO_2 and MgO/TiO_2 was around 20 nm.

References:

1. C. Y. Zhao, A. Krall, H. L. Zhao, Q. Y. Zhang and Y. Li, *Int. J. Hydrogen Energy*, 2012, **37**, 9967.
2. Q. Y. Zhang, E. A. Ackerman, M. Gajdardziska-Josifovska, H. L. Li and Y. Li, *Appl. Catal. A-Gen.*, 2011, **400**, 195.
3. L. L. Liu, H. L. Zhao, J. M. Andino and Y. Li, *ACS Catal.*, 2012, **2**, 1817.
4. W. N. Wang, W. J. An, B. Ramalingam, S. Mukherjee, D. M. Niedzwiedzki, S. Gangopadhyay and P. Biswas, *J. Am. Chem. Soc.*, 2012, **134**, 11276.
5. H. S. Jung, J. K. Lee and M. Nastasi, *Appl. Phys. Letters*, 2006, **88**, 0131071.
6. Y. Kohno, H. Ishikawa, T. Tanaka, T. Funabiki and S. Yoshida, *Phys. Chem. Chem. Phys.*, 2001, **3**, 1108.
7. G. S. Hu, L. Zhu, A. P. Jia, X. Hu, G. Q. Xie, J. Q. Lu, and M. F. Luo, *Appl. Spectroscopy*, 2012, **66**, 122.
8. D. Cornu, H. Guesmi, J. M. Krafft, and H. Lauron-Perno, *J. Phys. Chem. C*, 2012, **116**, 6645.